ATLAS Internal Note
INDET-NO-159
24 February 1997

Radiation Hardness of Silicon Detectors: Current Status

R. Wunstorf, *Member, IEEE*
Universität Dortmund, 44221 Dortmund, Germany

Invited Paper
presented at the
IEEE Nuclear Science Symposium 1996
Anaheim, California
November 2-9,1996

accepted for publication in the conference issue of the
IEEE Transactions on Nuclear Science
(June 1997)

Radiation Hardness of Silicon Detectors: Current Status

R. Wunstorf, *Member, IEEE*
Universität Dortmund, 44221 Dortmund, Germany

Abstract

Silicon detectors are used or going to be used as tracking devices in many high energy physics experiments. Therefore they are located close to the interaction point, where the detectors are exposed to very high particle fluxes and ionization doses, especially in future experiments with very high energies and luminosities. Ongoing investigations concerning the radiation damage, started already several years ago, include bulk and surface damage related questions. The two main objectives of these studies are: 1. Predict the radiation induced change in the detector parameters expected for any application, and 2. Improve the radiation hardness of the detectors.

A general overview of the current progress of the radiation hardness studies towards these goals is given here.

I. Introduction

Because of the very good tracking performance of silicon detectors, they are the first choice for many ongoing and future high energy physics experiments. Due to the increasing energy and luminosity of these experiments, the silicon detectors will be operated in a harsh radiation environment, with particle fluences up to several 10^{14} cm^{-2} and ionization doses of up to hundreds of KGy.

For silicon detectors two different radiation damage effects have to be distinguished. One is bulk damage, which is caused by the non-ionizing energy loss of penetrating particles and results in crystal defects. The other effect caused by ionization in the passivation layers at the surface of the detectors is summarized under the name surface damage. While bulk damage is a question of the silicon crystal, surface damage and how it affects the detector performance depends on the detector design and the processes used in the production.

In addition to these generic issues on radiation damage, especially for the usage of silicon detectors in an experiment, it is important to find out what are the crucial detector parameters for a particular application. This depends on the environment, e.g. particle composition and fluence, and conditions, such as temperature and time, in which the detectors are used. For example, the temperature conditions under which the detector is kept during and after irradiation are very important for the depletion voltage, as will be discussed later. Of particular interest in the context of quality assurance is to know the detector parameters which can be measured before the detectors are built into the experiment to give information about the behavior after irradiation, including e.g. the risk for breakdown. Information on these questions is important by itself, but in addition it provides the direction to proceed towards more radiation-hard detectors.

II. Bulk Damage

A. General Characteristics

While in the silicon crystal itself ionization is a reversible process, and therefore does not cause any damage, the energy transfer to crystal atoms which is the non-ionizing energy loss of the incident particle causes displacement damage. The primary defects are interstitials and vacancies, which can combine to form more stable defects, e.g. with impurities or to divacancies. If the energy transfer to the primary knock-on atom (PKA) is high enough, say over 2 KeV, so called 'clusters' will be produced, which are local highly disordered regions and behave differently from isolated point defects. For different incident particles, if the energy transfer is above the threshold for production of point defects and clusters, implying the same mixture of defects, the damage scales with the non-ionizing energy loss. This has been verified by comparing the irradiation induced changes in the detector parameters for different particles and particle energies [1,2,3].

Following particle interactions, neutrons, protons and pions with energies above 15 KeV produce cluster and point defects, where the relative number of point defects is higher for protons and pions due to the Coulomb interaction. On the other hand the energy transfer from electrons and gammas of up to more than 5 MeV is not high enough to produce cluster damage. Therefore electron- and gamma-induced damage is not expected to scale with the non-ionizing energy loss, and this is seen in the lower radiation-induced change of the detector parameters and in the different relative defect concentrations [1,4,5]. In most applications the expected bulk damage, dominantly caused by neutrons and charged hadrons, does scale with the non-ionizing energy loss and is therefore characterized in terms of equivalent fluence of 1 MeV neutrons.

B. Detector Parameter

The detector parameters which need to be addressed concerning bulk damage are the change in the effective impurity concentration and correspondingly the depletion voltage, the increase in leakage current and the increase in the charge collection deficiency.

The depletion voltage V_{depl}, which is defined by the electrically active impurities in the crystal, is an important parameter because it defines the minimum operating voltage for the space charge region to extend over the whole detector depth d and thus for full charge collection. From the measured depletion voltage the difference between donor and acceptor concentration, N_D and N_A, called the effective impurity concentration,

$$N_{eff}=N_D-N_A \tag{1}$$

can be calculated by

$$N_{eff}=\frac{2\cdot\varepsilon\cdot\varepsilon_0}{q_0\cdot d^2}\cdot V_{depl} \tag{2}$$

with $\epsilon\epsilon_0$ the permittivity in silicon, q_0 the elementary charge and

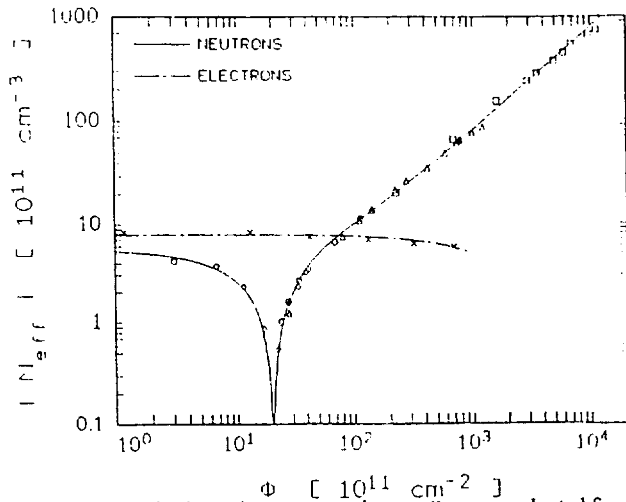

Figure 1a: Effective impurity concentration vs. fluence evaluated from C-V measurements of Si-detectors [1].

d the detector thickness. The effective impurity concentration (Fig. 1a) measured as function of the particle fluence for n-type starting material shows a decrease until the depletion voltage is almost zero, indicating intrinsic material. Towards higher fluences it increases again, showing a linear increase of acceptor like defects [1,2,6]. This dependence can be described by

$$N_{eff}(\Phi)=N_{D,0}e^{-c_D\Phi}-N_{A,0}e^{-c_A\Phi}-b\Phi \qquad (3)$$

where the first and the second term describe a donor and acceptor removal resp. from the starting donor concentration $N_{D,0}$ and acceptor concentration $N_{A,0}$ resp. with removal rates c_D and c_A and b is the rate of a radiation-induced acceptor increase.

The behavior at low fluences which is dominated by donor and acceptor removal has also been observed with 4-point probe measurements of silicon wafers [7] which is only sensitive to thermally ionized levels. A linear increase of the acceptor concentration at high fluences was not observed, indicating that the energy levels of these defects are deep in the band gap. This study on the silicon material itself, described in Ref. [7], also allowed a direct measurement of the donor removal rate c_D= $2.41\cdot 10^{-13}$cm^2 of Phosphorus, and gave an acceptor removal rate of c_A= $1.98\cdot 10^{-13}$cm^2.

The time dependence of the depletion voltage, especially the long term annealing effect first observed in 1992 in Ref. [1], has proven to be very important for the operation of irradiated detectors. The annealing behavior observed at room temperature and at 0 °C is shown in Fig. 1b. With time constants in the range of days a decrease of the radiation-induced change occurs soon after irradiation. At room temperature an increase in acceptor states appears about two weeks after irradiation, which leads to an increase of the depletion voltage, and is therefore sometimes called reverse annealing. This long term annealing effect is caused by radiation-induced defects which are not electrically active themselves, but when they anneal combine to form a defect which is now electrically active and causes the observed time dependent change [1]. This long term effect has been studied in their time and temperature dependence [8, 9]. It has been shown to be a second order process and can be suppressed by cooling the detector after irradiation [8] as shown in Fig. 1b for 0 °C. The generation rate of these defects is 0.05 cm^{-1} and is a limiting factor for long term applications in high fluence regions. Therefore it has to be foreseen to cool the detectors during and after operation periods and minimize the warm-up periods to a few days per year.

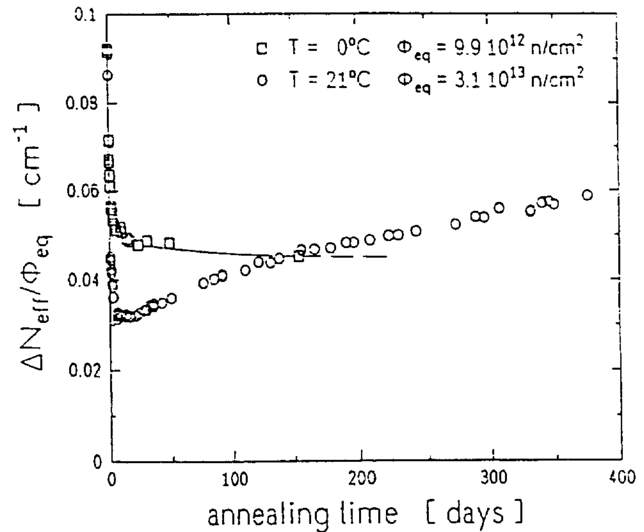

Figure 1b: Annealing behavior of the radiation-induced change of the effective impurity concentration at different temperatures. [8]

The increase of the leakage current due to irradiation induced generation centers is of importance in two respects, one the increased noise and the other the power consumption, which can even lead to thermal runaway [10]. Therefore, controlling the leakage current also requires cooling, but here mainly during operation. As shown in Fig. 2a a linear increase with a damage constant of α= $8\cdot 10^{-17}$ Acm^{-1} at room temperature without any annealing is observed as long as the material is not inverted. After type inversion an additional contribution appears with linear fluence dependence, but it shows a faster annealing, so that it is not seen after long irradiations [1].

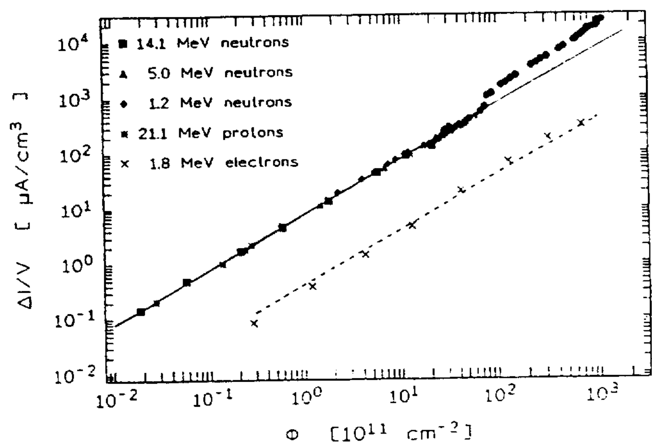

Figure 2a: Bulk generation current increase vs. fluence evaluated from I-V measurements of Si-detectors [1].

The observed room temperature annealing for the leakage current before type inversion shows a decrease which can be described with several exponential functions, leading over a year to about 1/3 of the current without annealing. The annealing factor is given by

$$g(t)=\sum a_i \cdot e^{-\frac{t}{\tau_i}}, \qquad \sum a_i = 1 \tag{4}$$

with the time constants τ_i and amplitudes a_i given in Tab. 1.

Table 1: Annealing parameter of the damage induced bulk generation current [1]

Time constant τ_i [min]	Relative amplitude a_i
$(1.78 \pm 0.17) \cdot 10^1$	0.156 ± 0.038
$(1.19 \pm 0.03) \cdot 10^2$	0.116 ± 0.003
$(1.09 \pm 0.01) \cdot 10^3$	0.131 ± 0.002
$(1.48 \pm 0.01) \cdot 10^4$	0.201 ± 0.002
$(8.92 \pm 0.59) \cdot 10^4$	0.093 ± 0.007
∞	0.303 ± 0.006

Taking the annealing into account for long term applications the bulk generation current can be calculated with a damage constant of $3 \cdot 10^{-17}$ Acm^{-1}. Higher temperatures accelerate the current decrease and lower temperatures slow it down. Fig. 2b shows good agreement among the annealing measurements for various temperatures T rescaled to the reference temperature T_R=20 °C using the time axis $\tau=\theta(T)\cdot t$, with

$$\Theta(T)=\exp(\frac{E_I}{k_B}\cdot[\frac{1}{T_R}-\frac{1}{T}]) \tag{5}$$

Therefore the expected current increase at the temperature T can be calculated as

$$\frac{\Delta I}{V}(\Phi,t,T)=\alpha\cdot\Phi\cdot g(\Theta(T)\cdot t)\cdot r(T) \tag{6}$$

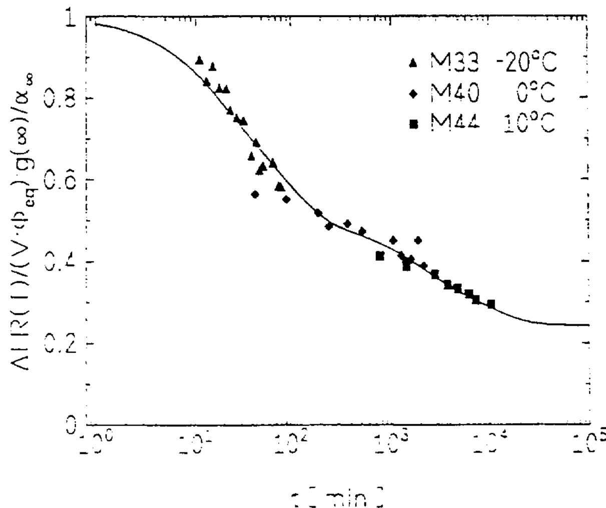

Figure 2b: Annealing behavior of the irradiation induced change of the current for different temperatures [11] compared to the annealing function for 20 °C [1] (solid line) on a rescaled time. [12]

where $r(T) = I(T)/I(T_R)$ describes the well-known temperature dependence of the bulk generation current.

The charge trapping, investigated separately for electrons and holes (Fig. 3), shows the same linear increase up to a fluence close to type inversion. While hole trapping still increases with the same rate of $0.26 \cdot 10^{-6}$ cm^{2}s^{-1}, there is another contribution to the electron trapping causing a slope of $1.01 \cdot 10^{-6}$ cm^{2}s^{-1} [1]. With these numbers the charge collection deficiency calculated for minimum ionizing particles (mips) agrees with the data from charge collection measurements with a beta source [2].

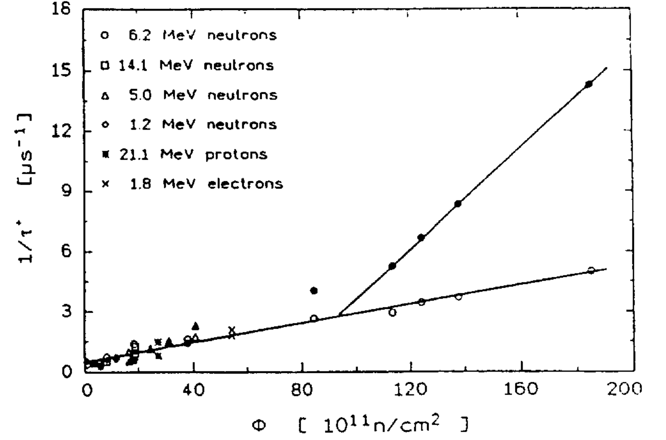

Figure 3: Trapping time constant for electron trapping (closed symbols) and hole trapping (open symbols) vs. fluence [1].

All these irradiation-induced changes of the detector parameters due to bulk defects, depletion voltage, current and charge collection deficiency, have been confirmed in many experiments and are now the basis on which predictions for a specific application are calculated. As an example Fig. 4 shows the changes expected over 10 years of operation for the silicon detectors in the ATLAS experiment at the LHC (CERN, Geneva), if the detectors are constantly maintained at 0 °C. This, of course, is not possible in a real experiment, although it would be ideal, especially, with regard to the long term annealing behavior of the depletion voltage (Fig. 1b).

For a real operational prediction some maintenance periods during which the whole experiment has to be warmed-up have to be considered. This was first discussed in Ref. [8] and taken into account in calculations of several operational scenarios, e.g. in Ref. [12,13]. As shown in Fig. 4 [12] the detector depletion voltage, for example at a 30 cm radius after 10 years of operation at 0 °C without any warm-up will be 270 V. With very short warm-up periods (20 °C) of only 3 days every year the depletion voltage will only increase to 300 V after 10 years, but with warm-up periods of one month every year the depletion voltage will reach 460 V.

Since the number of active defects created during such a warm-up period is determined by the number of inactive defects which have already been accumulated during the preceding irradiation periods, warm-up periods are less damaging to the detector performance at the beginning of an experiment than after a high accumulated fluence.

The operational predictions of the charge collection for mips calculated from the trapping time constants for electrons and holes

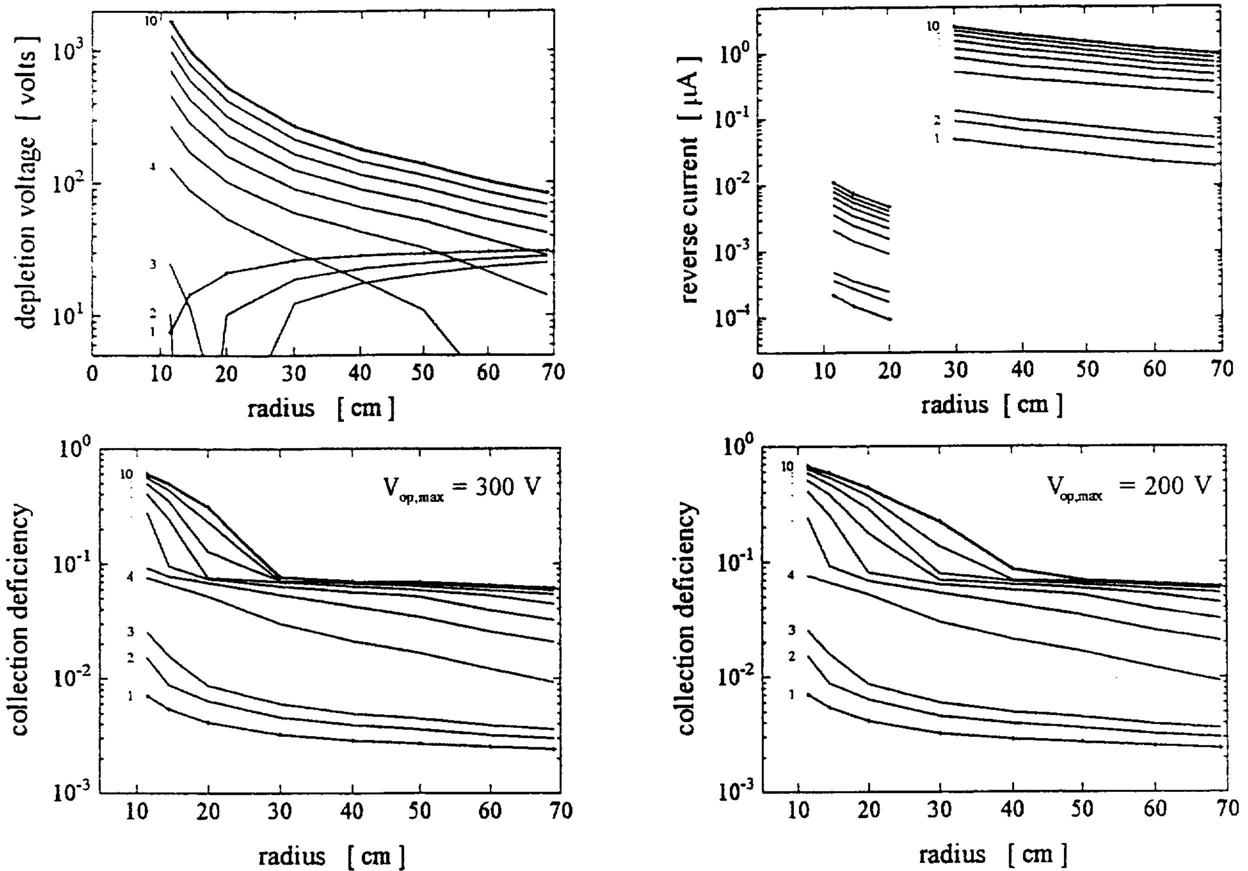

Figure 4: Example of operational prediction of the depletion voltage (300 µm detector thickness), the current (radii < 20 cm: 50 µm x 300 µm pixel detectors; radii >30 cm: strips with 112.5 µm x 12 cm) and charge collection deficiency at 200 V and 300 V maximum operating voltage, respectively. The calculations are for 10 years of operation of the ATLAS experiment at the LHC at CERN, assuming an integrated luminosity of 3 years at 10^{33} $cm^{-2}s^{-1}$ and 7 years at 10^{34} $cm^{-2}s^{-1}$. [12]

is shown in Fig. 4 for two different maximum operating voltages, $V_{op,max}$ = 300 V and $V_{op,max}$ = 200 V. As long as the depletion voltage is more than 50 V lower than the maximum operating voltage the charge collection was calculated for $V_{op} = V_{depl} + 50$ V, with a minimum operating voltage of V_{op} = 100 V. The sharp bend seen after more than 5 years of operation for smaller radii indicates the point where the Si-detectors become partially depleted due to the upper limit assumed for the operating voltage. Without this limit on the operating voltage, the only contribution to the charge collection deficiency is charge trapping which is always less than 10% reduction of the total charge. The effect of high charge collection deficiencies due to depletion voltages higher than the maximum operating voltage emphasizes again the importance of the long term annealing effect of the effective impurity concentration.

B. Correlation with Defects

Now that the radiation induced changes of the detector parameters can be calculated, the next question is: What are the defects in the silicon crystal which cause those changes and how can their creation be suppressed? Two main courses are being pursued to find hints to answer this question, which would have an important impact in the application of silicon detectors in high radiation environments. One is to study the radiation damage behavior of silicon bulk material which differs from the standard high resistivity detector grade, float-zone material, mainly produced by *WACKER Chemietronic* or *TOPSIL*. The other path, interconnected with the study of other materials, is the application of defect characterization methods to measure important defect parameters, such as energy levels in the gap, cross-sections and generation rates, which help to identify the defects.

A crystal growth process very different from the standard float-zone is epitaxial growth, which is used mostly in the electronic industry for thin, homogeneous, lower resistivity layers on top of a base material. The first study of epitaxial silicon is the comparison of the damage-induced changes with those observed for standard float-zone material. However, it could be more important, that the epitaxial process includes very different possibilities to dope the material with different impurities. For radiation damage studies, silicon detectors were manufactured from an epitaxial material with a thick epitaxial layer of 120 µm and a resistivity of about 1 kΩcm grown on low resistivity Czochralski silicon and their behavior studied [14]. The first results from this study of the depletion voltage versus fluence show a higher fluence for type inversion, possibly due to a difference in the donor and acceptor concentrations. With a sample irradiated with protons up to $1.5 \cdot 10^{14}$ cm^{-2} a smaller acceptor increase during long term annealing was observed, but another sample irradiated up to $3.5 \cdot 10^{14}$ cm^{-2} shows the same acceptor increase during long term annealing as standard float-

zone material. Further investigation will continue with epitaxial material, including samples from different epitaxial processes.

As mentioned in the last section, only shallow impurity levels can be measured with the 4-point probe method. Therefore, it is an important piece of information that the increase of acceptor states during long term annealing has also been seen using this method [7]. The same study, looking at silicon from special processes, also found a correlation of the number of defects created during long term annealing with the estimated boron concentration, which makes boron a possible candidate responsible for this long term annealing effect.

In the realm of defect characterization several different methods have been introduced over the last few years for the study of bulk defects in silicon detectors (Tab. 2). All methods have in common that they look to the transient behavior of a parameter, or the parameter itself in the case of TSC, during a temperature scan from as low as ~10 K up to room temperature, after filling the traps at the lowest temperature.

Table 2: Defect characterization methods employed for radiation damage studies of silicon detectors

Parameter Used	Defect Characterization Method		References
Capacitance	C-DLTS	Capacitance Deep Level Transient Spectroscopy	e.g. [15,16]
Current	I-DLTS	Current Deep Level Transient Spectroscopy	e.g. [17]
	TSC	Thermally Stimulated Current	e.g. [15,17,18]
Charge	TCT	Time resolved Current Transient	e.g. [19,20]
	TChT	Time resolved Charge Transient	e.g. [20,21]

The aim of these microscopic measurements is to identify the defects responsible for the radiation-induced changes seen in the macroscopic parameters. Knowing the responsible defects will give a direction for defect engineering, e.g. special changes to the material, such as introducing a given impurity, which can decrease the introduction rate of the responsible defect or compensate it. The first step towards this final goal of producing more radiation-hard silicon is a thorough study of the defects.

Fig. 5 shows an example of DLTS measurements, where the DLTS spectrum of a neutron irradiated sample is compared with the spectrum of a sample which was irradiated with gammas from a ^{60}Co source. Since the difference of the two spectra is due to the fact that the energy transfer of the gammas to the crystal atoms is too low to produce cluster defects, their comparison enables conclusions to be drawn about the role of different kind of defects in clusters and point defects.

In the comparison of the DLTS spectra it is striking that the levels E7 and E8-a are not found in the ^{60}Co-γ irradiated samples. Both defects are electron traps, and the parameters of these defects are measured, however they are not yet identified in their crystal structure. Most likely they are related to higher order vacancy and

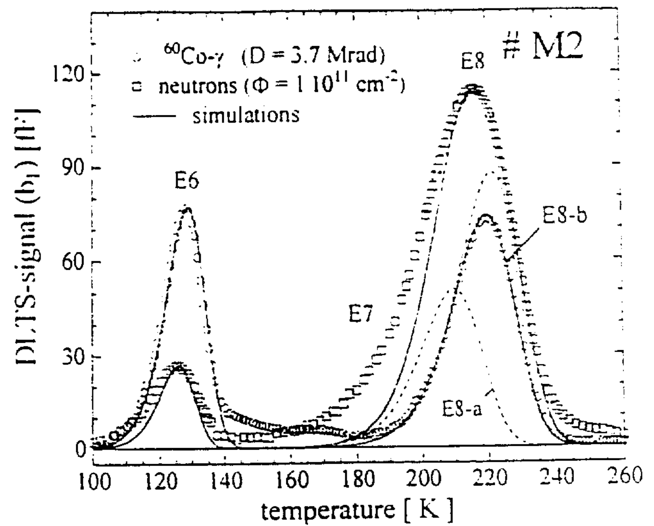

Figure 5: Comparison of DLTS-spectra measured after neutron and gamma irradiation [5].

interstitial defects, which are formed in connection with clusters [5].

The ratios of the generation rates of the defects after neutron and gamma irradiation are summarized after Ref. [5] in Tab.3 and give further indications of the differences between cluster defects and point defects. For example the ratio of the concentration of vacancy-related defects (vacancy-oxygen [VO] and double vacancy [VV]) to interstitial-related defects (carbon-carbon [CC] and carbon-oxygen [CO]) is higher in neutron irradiated samples than the expected 1:1, possibly due to higher order vacancy defects in clusters. This also corresponds to the fact that the

Table 3: Ratios of the generation rates of defects in neutron and ^{60}Co-γ irradiated samples as measured with DLTS and some interpretations [5]

Ratios of generation rates	Neutron irradiation	^{60}Co-γ irradiation	Interpretation
$\frac{[CO]}{[CC]}$	3.5	3.2	type of irradiation has no influence on migration of C_i
$\frac{[VO]}{[VV]}$	0.8	35	n-irrad.: many V produced by one PKA (VV creation possible)
$\frac{[VO]}{[CC]+[CO]}$	0.4	0.9	n-irrad.: more V than I are captured in primary damage region
$\frac{[VO]+2\cdot[VV]}{[CC]+[CO]}$	1.36	1.0	γ-irrad.: ratio of V related to I related defects is 1:1
$\frac{[VV^{(-/0)}]}{[VV^{(=/-)}]}$	3.4	1.0	n.-irrad.: VV are mostly localized in disordered regions

relative number of double vacancies produced by neutrons is already more than 13 times higher than after gamma irradiation.

Another interesting point is the concentration ratio measured for the two charge states of the double vacancy $VV^{(-0)}$ and $VV^{(=-)}$ which is 1 as expected in the case of gamma irradiation, but 3.4 after neutron irradiation. Since both levels belong to the identical defect, this means that the lower level of the double vacancies are suppressed if the defect is located in a cluster or at its edge. Fig. 6 shows DLTS spectra measured in the temperature range of the double vacancies, after different annealing steps. The peak for the $VV^{(=-)}$ at lower temperatures is much smaller than the peak for $VV^{(-0)}$ at ~ 225 K. During a series of 10 minute isochronal annealing steps from 50 °C to 210 °C the latter peak decreases, with two annealing stages at 70 °C and 170 °C, leaving the final peak of the $VV^{(-0)}$. The defects which correspond to those annealing stages are not yet identified, but possible candidates are higher order vacancy defects, as the two stages are not found after gamma irradiation. Of special interest concerning macroscopic detector parameters, is the observation that the current behavior during the isochronal annealing shows a correlation with the concentration of the two defects which anneal out. As seen in Fig. 6, the visible concentration of the $VV^{(=/-)}$ defect increases during this annealing procedure [22].

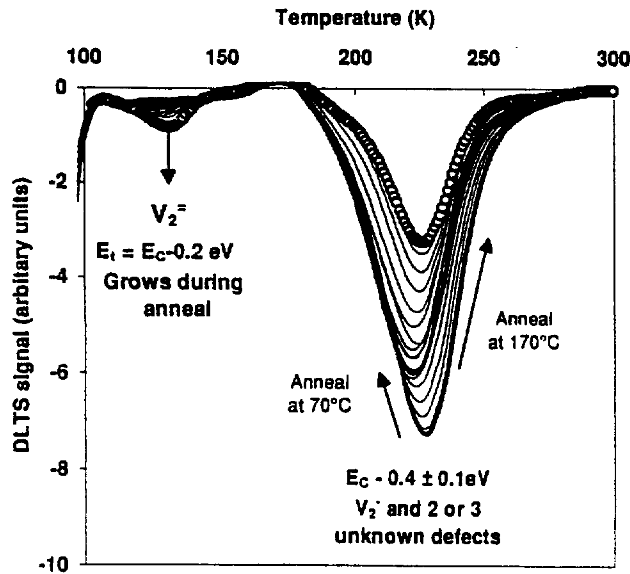

Figure 6: DLTS spectra of the two charge states of the double vacancy $VV^{(=-)}$ and $VV^{(-0)}$ [18] during isochronal annealing from room temperature to 210 °C.

Two reasons have been proposed to explain this abnormal behavior of a suppressed $V^{(=-)}$ peak in DLTS spectra, one a bonding distortion due to lattice strain in a cluster [23], the other a direct carrier transition which can happen between closed defects in clusters [22]. This example also shows that clusters play a significant role, but up to now little is known about their structure and the mechanisms by which they affect the detector parameters, e.g. by a factor 20 in the bulk generation current (see Fig. 2a). Likewise these differences are clear in Ref. [4], where an attempt is made to describe the gamma-induced and the neutron-induced damage within a defect kinetics model based on the generation rates of V and VV defects.

In standard detector grade silicon the impurity concentrations are very low, and for most impurities below the detection limit of available analytical methods, however oxygen and carbon related defects are important as seen in Tab. 3 for example. Worth mentioning in this context is the ROSE collaboration [24] which has as its goal the development of more radiation-hard silicon detectors, and includes almost all groups working world-wide in this field. To investigate the role of oxygen and carbon related defects, the ROSE collaboration has been successful in obtaining special grown silicon with higher oxygen content, which is currently under investigation.

III. SURFACE DAMAGE

A. Basic Effects

In contrast to the radiation-induced crystal defects in the bulk, the term surface damage summarizes all radiation-induced effects in the surface passivation layers, in most cases silicon dioxide, and at their interfaces such as the Si/SiO_2 interface. Besides the location, bulk and surface effects are also distinguishable by their causes. While crystal damage is due to the non-ionizing energy loss, the surface damage is caused by ionization within the passivation layers and charges trapped in the layers or at the interfaces. The effect of displacement damage, which also happens in the passivation layers is negligible.

The electrons and holes created by ionizing radiation passing through the passivation layer have a high probability for immediate recombination, especially if no electric field is applied. With higher electric field strength the number of free charges increases. Because of their high mobility electrons are swept out almost immediately leaving the much slower holes behind. Depending on the direction of the electric field, more or less holes move to the Si/SiO_2- interface where they are trapped, causing two basic surface damage effects: 1. An increase of the oxide charge N_{ox}, and 2. The introduction of surface generation centers, which are responsible for higher surface velocity.

The positive oxide charges cause an electron accumulation underneath the interface and therefore a higher voltage is needed to achieve the flatband condition, leading to an increase of the flatband voltage of

$$\Delta V_{FB} = \frac{q_0 \cdot d_{ox}}{\varepsilon \cdot \varepsilon_0} \cdot \Delta N_{ox} \tag{7}$$

with d_{ox} the oxide thickness, ΔN_{ox} the increase of the number of oxide charges q_0 the elementary charge. Fig. 7 shows the radiation-induced increase of the flatband voltage versus the bias applied during irradiation, reflecting the described mechanism. This was measured with MOS structures on n-type detector grade silicon with a 220 nm oxide grown in an oxidation process typical for detectors [26].

Knowing this dependence of the radiation-induced surface effect on the applied bias during irradiation, the change of the flatband voltage and the surface generation current have been measured for both cases as shown in Fig. 8a and 8b. As measured in electronic-device related studies of surface effects, saturation is also found for silicon detectors for the basic radiation-induced

surface effects, with a saturation value for the oxide charge of several 10^{12} cm^{-2} [28,29].

B. Consequences on Detector Design and Processing

Concerning the relevance of these radiation-induced changes to detector performance, it is important to study their influence on the detector parameters. In addition to measurements of test devices, device simulation is an important tool to understand the behavior of different designs under ionizing radiation. Fig 9 shows, as one example, the simulation of the electron concentration, taking into account the radiation-induced oxide charge according to the electric field in the oxide during irradiation. The electron accumulation at the points with a high electric field during irradiation explains, what was first found with proton micron beam investigations of this structure as small dead regions underneath these points [25, 27].

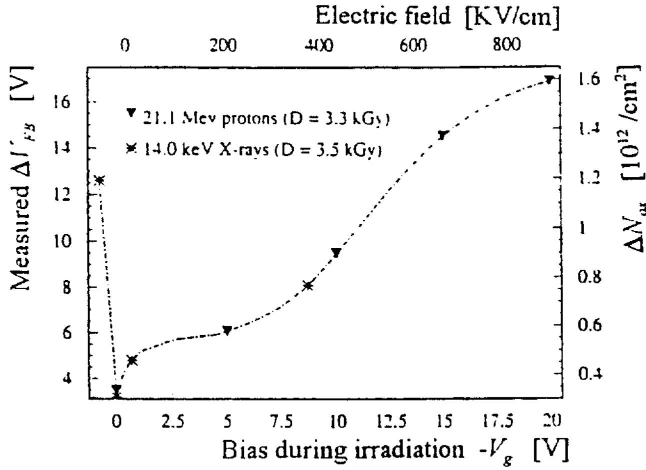

Figure 7: Radiation-induced flatband voltage increase vs. bias voltage applied during irradiation. [1,25]

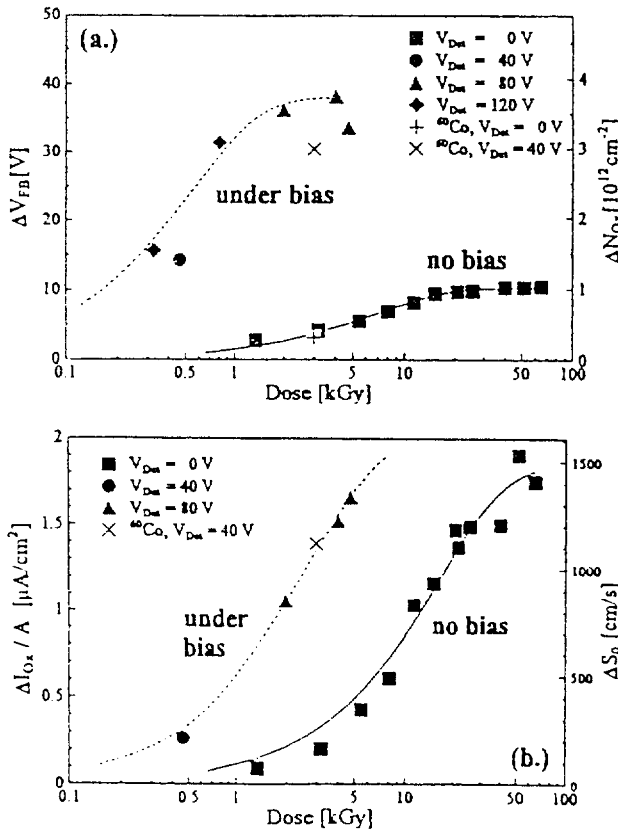

Figure 8: Increase of flatband voltage resp. oxide charge (a.) and surface generation current resp. surface velocity (b.) vs. ionizing dose. [27]

For finely segmented structures, e.g. strip detectors, the surface damage has also an effect on the depletion voltage, due to the electron accumulation underneath the Si/SiO_2-interface in the gap between the strips [30]. As the simulation for 50 µm pitch in Fig. 10 shows, the depletion voltage is higher for smaller strip width, or wider gaps. This effect is relatively small for the case before ionizing irradiation ($\Delta V_{ox}=2 \cdot 10^{11}$ cm^{-2}), but is significantly larger after irradiation, where in saturation ($\Delta V_{ox}=3 \cdot 10^{12}$ cm^{-2}) the additional voltage required for wide gaps is 25 V for an oxide thickness of 0.22 µm (Fig. 10a). This number increases significantly for thicker oxide (Fig. 10b) or if the gate boundary condition can not be applied and the von Neumann boundary condition exists [30]. The gate on top of a thinner oxide builds a MOS structure, helping to deplete the electron accumulation underneath the interface.

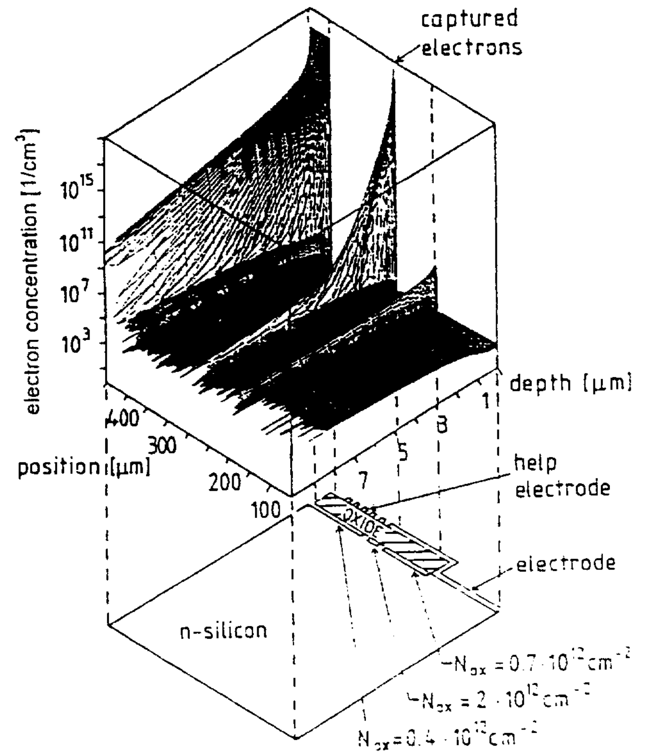

Figure 9: Electron concentration after ionizing irradiation, simulated for a detector with electrode overlap for 80 V bias voltage during irradiation. [25]

The choice of small gap or wide gap is first of all determined by the application, e.g. if charge sharing or charge focusing on one strip is desired. As well as the consequence on the depletion voltage after irradiation (Fig. 10), account has to be taken also of the peaks in the electric field occurring at the edges of the implant and which are significantly higher in wide gap designs [30]. Up to now it is not known how high the electric field can be without taking any risk for breakdown. This needs more investigation, especially as this risk may be connected to other design questions

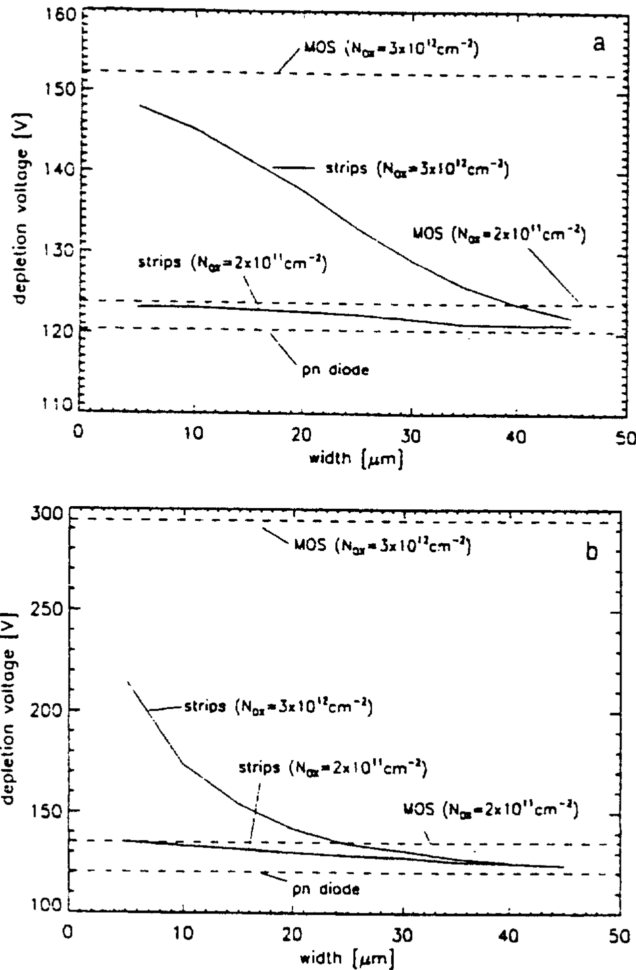

Figure 10: Depletion voltage vs. strip width for oxide charges before (N_{ox}= 2·10^{11} cm^{-2}) and after irradiation (N_{ox}= 3·10^{12} cm^{-2}) for an oxide thickness of (a) 0.22 μm and (b) 1.22 μm. (Wafer thickness: 280 μm; Strip pitch: 50 μm) . [30]

and to the processing. Since peaks of high electric fields imply a higher risk, it is important to minimize them as far as possible.

Another important parameter for strip like geometries is the interstrip capacitance, which contributes significantly to the total capacitance. Measurements on the irradiation induced change of the interstrip capacitance for the p-side and the n-side of a double sided detector have been studied, e.g in [31, 32, 33]. First of all it can be established that the strips on the p-side are not shorted, even after the bulk inverted to p-type. This can be explained by a thin n-type layer at the surface, which does not convert to p-type, as first suggested in Ref. [1]. It was found that all measurements of the conduction type concerning the bulk show type inversion and all measurements looking for the conduction type right at the surface still show n-type, even after very high fluences. The change of the interstrip capacitance due to irradiation is not dramatic. Essentially no change due to γ-irradiation and only small changes due to proton irradiation: On the p-side an increase of below 1 pF and on the n-side a decreases of ~1 pF was observed for various gap sizes after proton irradiation up to 10^{14} p/cm^2.

Other surface effects have to be taken into account when designing silicon detectors to be used in a harsh radiation environment. Depending on the design, some effects are not important, but each structure used has to be tested for radiation hardness. For example, the punch-through biasing structure, used in some designs for ac-coupled detectors [34], when irradiated up to the saturation of the surface defects shows an increase of the required punch-through voltage of up to 15 V.

Another crucial issue is the breakdown behavior seen in the current characteristic and/or as micro discharge [35]. Guard ring structures [36, 37, 34] are important in this context since they are needed to minimize the risk at high operating voltage due to bulk damage after higher fluences. A multi guard ring structure is now often used to distribute the voltage drop over several steps. Fig. 11 shows the potential of the individual guard rings under a worst-case condition, where the bias voltage of 100 V is applied directly to the outermost ring no. 1. This measurement shows no

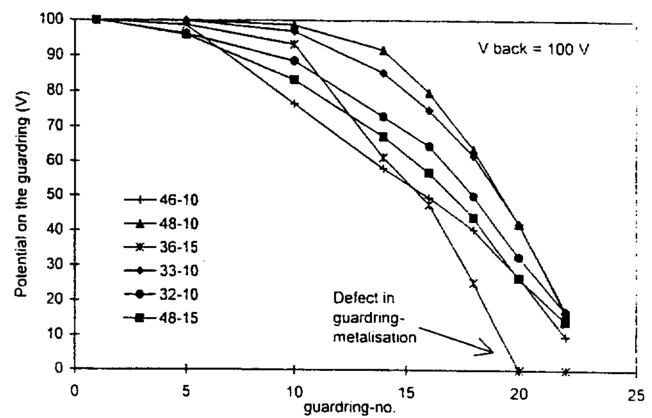

Figure 11: Potential drop from detector edge to strip region on a multi guard ring structure on the p-side in the worst-case scenario of applying the bias voltage (100 V) directly to the outermost guard ring no. 1. (φ= 0 - 4.25·10^{13} cm^{-2}, 24 GeV protons) [34]

significant change with irradiation, even through type inversion. This means that it is possible to measure the performance of the guard ring structure already in the unirradiated case. For example in the design with equal distances between the rings (Fig. 11), it is found that the inner guard rings have to hold a higher voltage drop. This can be adjusted by spacing the rings accordingly.

IV. Conclusions

An overview of the important bulk defects and an introduction to ongoing studies of defect characterization is given in the first part of this review. The aim of these studies is to develop more radiation-hard silicon, which can be used for applications in harsh radiation environments. The design dependent surface effects described in the second part can only give an introduction to the relevant questions. More systematic studies of the influence of certain design parameters on radiation hardness are needed. Since the surface effects are especially sensitive to the structure of the Si/SiO_2-interface, they depend on process parameters, e.g. the oxidation, as well. This is one of the questions to be investigated in the future.

V. References

[1] R. Wunstorf, Ph.D thesis, Universität Hamburg, DESY-

FH1K-92-01 (1992)

[2] S. Bates at al., Pion-induced damage in silicon detectors, Nucl. Instr. and Meth. A379 (1996).

[3] H. Feick et al., Long term damage studies using silicon detectors fabricated from different starting materials and irradiated with neutrons, protons, and pions, Nucl. Instr. and Meth. A377 (1996)

[4] B.C. McEvoy, Defect evolution in silicon detector material, ROSE/TN/96-1 (1996), submitted for publication.

[5] M. Moll et al., Comparison of defects produced by fast neutrons and ^{60}Co-gammas in high resistivity silicon detectors using Deep Level Transient Spectroscopy, Contrib. to the Intern. Conf. on Radiation Effects on Semiconductor Material, to be published in Nucl. Instr. and Meth.

[6] D. Pitzl et al., Type inversion in silicon detectors, Nucl. Instr. and Meth. A311 (1992)

[7] R. Wunstorf et al., Investigation of donor and acceptor removal and long term annealing in silicon with different boron/phosphorus ratios, Nucl. Instr. and Meth. A377 (1996)

[8] E. Fretwurst et al., Reverse annealing of the effective impurity concentration and long term operational scenario for silicon detectors in future collider experiments, Nucl. Instr. and Meth. A342 (1994)

[9] H.-J. Ziock et al., Temperature dependence of the radiation induced change of depletion voltage in silicon PIN detectors, Nucl. Instr. and Meth. A342 (1994)

[10] T. Kohriki et al., First observation of thermal runaway in radiation damaged silicon detectors, IEEE Trans. on Nucl. Sci., Vol. 43, No. 3 (1996)

[11] F. Lemeilleur, private communication

[12] H. Feick et al., Radiation damage of Si-detectors and operational projections for LHC experiments, SiTP-TR-112, CERN, Geneva (1995)

[13] J.A.J. Matthews, Bulk radiation damage in silicon detectors and implications for LHC experiments, to be published in Nucl. Instr. and Meth.

[14] B. Dezillie et al., Experimental results on radiation induced bulk damage effects in float zone and epitaxial silicon detectors, Contrib. to the 5th Intern. Workshop on Vertex Detectors, Chia, Cagliari, Italy 1996, CERN-ECP/96-08

[15] E. Fretwurst et al., Neutron induced defects in silicon detectors characterized by DLTS and TSC methods, Nucl. Instr. and Meth. A377 (1996)

[16] V. Eremin et al., Detection mechanism of radiation induced defect levels in high resistivity silicon by DLTS method with preliminary filling pulse, to be published in J. Appl. Phys.

[17] C.J. Li and Z. Li, Development of current-based microscopic defect analysis methods and associated optical filling techniques for the investigation on highly irradiated high resistivity silicon detectors, Nucl. Instr. and Meth. A364 (1995)

[18] H. Feick et al., Analysis of TSC spectra measured on silicon pad detectors after exposure to fast neutrons, to be published in Nucl. Instr. and Meth.

[19] V. Eremin et al. Development of transient current and charge techniques for the measurement of effective impurity concentration in the space charge region of p-n junction detectors, Nucl. Instr. and Meth. A372 (1996)

[20] E. Fretwurst et al., Investigation of damage induced defects in silicon by TCT, to be published in Nucl. Instr. and Meth.

[21] V. Eremin et al., Transient Current Technique: a tool to analyze transport phenomena in irradiated silicon, Contr. to the Intern. Conf. on Radiation Effects on Semiconductor Material (1996)

[22] S.J. Watts et al., A new model for generation-recombination in silicon depletion regions after neutron irradiation, Contrib. to the IEEE Nucl. Sc. Radiation Effects Conf. 1996, ROSE/TN/96-2

[23] G. Svensson et al., Nucl. Instr. and Meth. B 80/81 (1993)

[24] ROSE Collaboration, RD48, CERN/LHCC 96-23, P62/LHC R&D (1996)

[25] R. Wunstorf et al., Simulation of irradiation induced surface effects in silicon detectors, to be published in Nucl. Instr. and Meth.

[26] J. Kemmer, Improvement of detector fabrication by planar process, Nucl. Instr. and Meth. A226:86 (1984)

[27] R. Wunstorf et al., Damage-induced surface effects in silicon detectors, Nucl. Instr. and Meth. A377 (1996)

[28] E.H. Nicollian and J.R. Brews, MOS - Physics and Technology -, Wiley, New York (1982)

[29] J.M. McGarrity at al., in G. Harbeke and M. Schulz (eds.) Semiconductor Silicon , Springer, Berlin (1989)

[30] R.H. Richter et al., Strip detector design for ATLAS and HERA-B using two-dimensional device simulation, Nucl. Instr. and Meth. A377 (1996)

[31] E. Barberis et al., Capacitances in silicon microstrip detectors, Nucl. Instr. and Meth. A342 (1994)

[32] E. Barberis et al., Analysis of capacitance measurements on silicon microstrip detectors, IEEE Trans. on Nucl. Sci., Vol. 41, No. 4 (1994)

[33] T. Rohe, Diploma thesis, Universität Dortmund (1996)

[34] C. Gößling et al. Irradiation tests of double-sided silicon detectors optimized for the ATLAS-inner-detector-region, Nucl. Instr. and Meth. A377 (1996)

[35] T. Ohsugi et al., Microdischarges of ac-coupled silicon strip sensors, Nucl. Instr. and Meth. A342 (1994)

[36] A. Bishoff et al., Breakdown protection and longterm stabilisation for Si-detectors, Nucl. Instr. and Meth. A326 (1993)

[37] B.S. Avset et al., The effect of metal field plates on multiguard structures with floating p^{+} guard rings, Nucl. Instr. and Meth. A377 (1996)